Journal of Power Sources 217 (2012) 449–458

Contents lists available at SciVerse ScienceDirect

Journal of Power Sources

journal homepage: www.elsevier.com/locate/jpowsour

Evidences of the migration of Pt crystallites on high surface area carbon supports in the presence of reducing molecules

Z. Zhao, L. Dubau [1], F. Maillard*,[1]

Laboratoire d'Electrochimie et de Physico-chimie des Matériaux et des Interfaces, UMR 5279 CNRS, Grenoble INP, Université de Savoie, Université Joseph Fourier, 1130 rue de la piscine, BP75, 38402 Saint Martin d'Hères Cedex, France

GRAPHICAL ABSTRACT

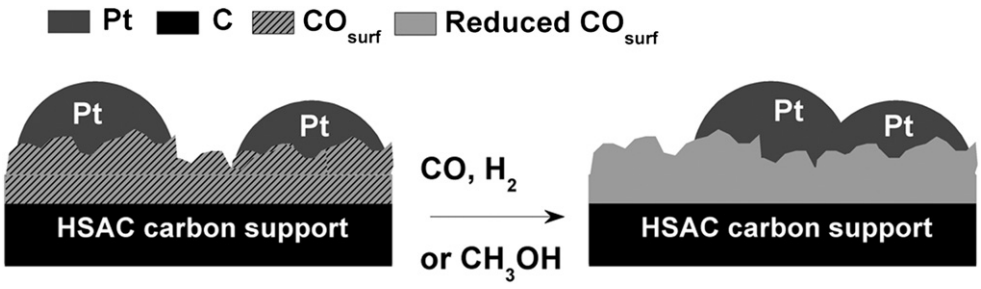

HIGHLIGHTS

- Evidences of the migration of Pt crystallites in the presence of H_2, CO or CH_3OH.
- The migration rate of the Pt crystallites is the largest in CO-containing solution.
- First insights into the interactions between Pt nanoparticles and carbon supports.

ARTICLE INFO

Article history:
Received 25 February 2012
Received in revised form
2 June 2012
Accepted 5 June 2012
Available online 13 June 2012

Keywords:
Proton exchange membrane fuel cell
Durability
Crystallite migration
Pt nanoparticles
Metal–carbon interactions

ABSTRACT

In this study, we made use of structural markers to gain more insights into the structural stability of commercial carbon-supported Pt electrocatalysts under oxidizing, inert and reducing atmospheres. The materials were characterized by electron microscopy and electrochemical techniques in the fresh state and after various aging conditions. The results show that Pt nanoparticles supported on Vulcan XC72 are not immobile but prone to agglomerate during potential sweeping in the presence of hydrogen (H_2), methanol (CH_3OH), and carbon monoxide (CO). The migration rate of the Pt crystallites is the largest in CO-containing solution and decreases in the order CO > CH_3OH > H_2. We postulate that the morphological changes of the Pt/C nanoparticles are related to the reduction of the oxygen-bearing carbon surface groups strongly interacting with the Pt metal phase.

1. Introduction

Conventional catalytic layers of proton-exchange membrane fuel cells (PEMFC) utilize Pt-based catalysts supported on porous carbon supports such as carbon blacks. Carbon blacks possess large surface area, high electron conductance, chemical inertness, adequate

* Corresponding author. Tel.: +33 476 82 65 88; fax: +33 476 82 67 77.
E-mail address: frederic.maillard@lepmi.grenoble-inp.fr (F. Maillard).
[1] ISE active member.

0378-7753/$ – see front matter © 2012 Elsevier B.V. All rights reserved.
http://dx.doi.org/10.1016/j.jpowsour.2012.06.016

porosity and low cost, which make them attractive for this application [1,2]. Yet, providing long-term stability to the Pt-based nanoparticles under PEMFC operating conditions has proven challenging. Degradations mechanisms of carbon-supported Pt-based nanoparticles include: (i) 3D Ostwald ripening, where the smaller crystallites dissolve preferentially, yielding the formation of Pt^{z+} and M^{y+} ions (M being the alloying element) and their redeposition onto larger crystals [3–6]; (ii) the chemical reduction of the Pt^{z+} ions in ion conductors, yielding formation of electrically disconnected Pt crystallites [7]; (iii) the corrosion of the carbon support leading to the detachment of the metal nanoparticles [8] and (iv) the migration of Pt crystallites [9–12]. The interest reader is referred to the comprehensive review of Shao-Horn et al. [9] for more details.

Although there is a large body of experimental evidences for the first three mechanisms, the migration of crystallites has only been seldom explored. There are several reasons for this, the most obvious being that crystallite migration, carbon corrosion, and Ostwald ripening are interdependent mechanisms or occur simultaneously [7,13]. Indeed, the corrosion of the carbon support to gaseous species induces the movement of the metal crystallites and their further agglomeration/detachment [14]. Similarly, the preferential dissolution of the smallest crystallites during Ostwald ripening is likely to influence their mobility on the carbon support. Another reason is that crystallite migration, carbon corrosion, and Ostwald ripening produce to some extent similar morphological changes (particle size growth, agglomeration and eventually coalescence of the metal particles) [7,14]. Several studies tried to make a distinction between a sintering caused by Ostwald ripening or by crystallite migration on the basis of the shape of the particle size distribution (PSD) [15]. However, such analysis is strongly dependent on the quality, the choice and the proper analysis of representative transmission electron microscopy (TEM) images and, practically speaking, remains hardly feasible.

Dealing with crystallite migration also raises the nature of the interactions existing between the metal nanoparticles and the underlying carbon support. There is a consensus in the scientific community to say that carbon surface oxides (referred to as CO_{surf} in what follows) play a major role during the synthesis of metal nanoparticles [16–25]. Lowde et al. [17] and Prado-Burguete et al. [18] argued that aqueous metal ion species strongly interact with the oxygenated groups present on the carbon support through electrostatic interactions and determine the structure and the morphology of the final crystallites (e.g. particle size distribution and degree of agglomeration). On the contrary, other authors [16,23] reported a decrease of the metal dispersion in the presence of oxygen-bearing surface groups. Now, the persistence of these interactions after the reduction of the metallic salt to form a metal nanoparticle remains a still open question. There are experimental evidences, from electron-spin resonance [26], X-ray photoelectron spectroscopy [19,27–31] and infrared spectroscopy studies [32,33], that metal nanoparticles interact with the carbon support via the oxygen atoms of CO_{surf} groups. This interaction not only influences the kinetics of PEMFC reactions [2] but also the resistance to sintering of the metal particles in both the gas [21,34] and the liquid phase [35]. On the other hand, CO_{surf} groups are generated on high surface area carbon supports (HSAC) in PEMFC operating conditions (low pH <1, high temperature >70 °C, high electrode potentials and oxygen-containing environment at the cathode) [36–38]. In an early study, Giordano et al. [39] showed that the presence of CO_{surf} groups on the carbon support enhances the carbon corrosion rate, and the latter was rationalized by the transfer of oxygenated species from the Pt nanoparticles to the CO_{surf} species, to form gaseous products, CO and CO_2 [14,37,40–42]. Summing up, CO_{surf} groups play a dual role: (i) they behave as anchoring sites for the metal nanoparticles, and (ii) they are reaction intermediates in the corrosion of the native carbon support. However, their interaction with the metal nanoparticles is still not fully understood and is the focus of the present study.

To reach this objective, commercial Pt/Vulcan XC72 electrocatalysts (denoted Pt/C in what follows) were aged in "mild" conditions, for which the corrosion of both the Pt nanoparticles and the carbon support cannot be considered dominant. Transmission electron microscopy and electrochemical techniques were successfully employed to characterize the fresh and the aged catalysts. We show that the migration of Pt crystallites is accelerated in the presence of "reducing" molecules such as H_2, CO, and CH_3OH.

2. Experimental

2.1. Physical characterization of the carbon supported Pt nanoparticles

Three samples based on Pt nanoparticles supported on Vulcan XC72 were investigated to explore the migration of Pt crystallites. They were supplied by E-Tek and have different weight fractions (wt.%) of 20, 30 and 40%, translating into surface averaged mean particle size of 2.9, 3.4 and 4.7 nm, respectively (see Table 1). The catalysts were used as-received without any further treatment.

2.2. High-resolution transmission electron microscopy imaging

The metal nanoparticles were examined with a Jeol 2010 TEM operated at 200 kV with a point to point resolution of 0.19 nm. The TEM images were used to build the particle size distribution of the catalysts before/after electrochemical treatment. From these observations, the particle size distribution, the number averaged diameter:

Table 1
Number and surface averaged mean particle size, density of isolated and agglomerated particles and loss of isolated Pt particles for three Pt/C commercial electrocatalysts before/after repetitive CO stripping voltammograms or after repetitive pseudo CO strippings voltammograms.

	20 wt.% Pt/C		30 wt.% Pt/C		40 wt.% Pt/C		
	Fresh	After 10 CO stripping voltammograms	Fresh	After 10 CO stripping voltammograms	Fresh	After 10 CO stripping voltammograms	After 8 pseudo + 2 real CO strippings
$\overline{d}_N$/nm	2.5	2.5	2.7	2.9	3.5	4.6	3.6
$\overline{d}_S$/nm	2.9	2.9	3.4	3.4	4.5	5.3	4.5
Number of isolated particles/μm^{-2} carbon	38,000	32,000	10,800	8000	8000	5600	7500
Number of agglomerated particles/μm^{-2} carbon	2500	2500	2800	3000	2600	2200	2200
Total number of particles/μm^{-2} carbon	40,500	34,500	13,600	11,000	10,600	7800	9700
Fraction of agglomerated particles/%	6.2	7.2	20.6	27.3	24.5	28.2	22.7
Loss of isolated particles/%	–	15.8	0	26.0	0	30.0	6.2

$$\overline{d}_N = \frac{\sum_{i=1}^{n} n_i d_i}{\sum_{i=1}^{n} n_i} \quad (1)$$

and the surface averaged diameter:

$$\overline{d}_S = \frac{\sum_{i=1}^{n} n_i d_i^3}{\sum_{i=1}^{n} n_i d_i^2} \quad (2)$$

were determined by eye-counting over ca. 400 particles (n_i stands for the number of particles having a diameter d_i). Only "isolated" particles (that is non-agglomerated, single grain spherical particles) were counted to build the PSD. We also used TEM images to evaluate the number of isolated/agglomerated particles per μm^2 of carbon, by eye-counting over typically 20 representative images.

2.3. Electrochemical measurements in liquid electrolyte

2.3.1. Solutions

All the glassware used in this study was cleaned by immersion in a H_2SO_4:H_2O_2 mixture overnight and thoroughly rinsed with MQ-grade water. Solutions were prepared from ultrapure water (MQ grade, 18.2 MΩ cm, 1–3 ppm TOC) and $HClO_4$ (Suprapur, Merck). The electrolyte was a 0.1 M $HClO_4$ solution purged with argon (99.99%).

2.3.2. Electrochemical cell set-up

The working electrode was a porous rotating disk electrode (RDE) composed of Pt/C 20, 30 or 40 wt.% (E-Tek) deposited on a glassy carbon disk (Sigradur, 0.196 cm^2) and immersed in the electrochemical cell at controlled electrode potential: $E = 0.10$ V *vs.* the reversible hydrogen electrode (RHE). The counter-electrode was a Pt foil and the reference electrode – a mercury sulfate electrode (MSE) $Hg|Hg_2SO_4|0.1$ M H_2SO_4 (aq) – connected to the cell via a Luggin capillary.

2.3.3. Preparation of porous rotating disk electrodes (RDE)

Porous RDE were prepared as follows. A mixture of 5.0 mg of Pt/C, 2.4 mL of MQ-grade water and 54 μL 5 wt.% Nafion® solution (Electrochem. Inc.) was ultrasonically treated for 30 min to obtain a well-dispersed ink. An aliquot was then deposited onto a glassy carbon disk and sintered for 5 min at $T = 383$ K to ensure its binding to the glassy carbon disk and evaporation of the Nafion® solvents.

2.3.4. Electrochemical characterization and durability tests

The electrochemical characterization and the durability tests on the Pt/C catalysts were conducted in two identical four-electrode cells thermostated at $T = 20$ °C. In the "characterization cell", the real surface area of the fresh/aged Pt/C electrocatalysts was determined using CO-stripping voltammograms. The CO saturation coverage was established by bubbling CO for 6 min and purging with Ar for 39 min, while keeping the electrode potential at $E = 0.1$ V *vs.* RHE. It was assumed that the electrooxidation of an adsorbed CO monolayer requires 420 μC cm^{-2}. After electrochemical characterization, the porous RDE was emerged at $E = 0.1$ V *vs.* RHE, transferred into the "durability test cell" and contacted at $E = 0.1$ V *vs.* RHE with the same supporting electrolyte saturated with H_2, CO or methanol. The durability test was performed in two parts, the first one consists of 50 potential cycles between 0.05 and 0.4 or 1.23 V *vs.* RHE at $v = 0.20$ V s^{-1}. The electrode was then emerged at $E = 0.1$ V *vs.* RHE, thoroughly rinsed with water and transferred back into the "characterization cell". After electrochemical characterization, the next 750 cycles were conducted following a similar procedure.

3. Results and discussion

3.1. Definition of structural markers of "crystallite migration"

During crystallite migration, crystallites collide, form agglomerates and eventually coalesce to form larger crystallites. Consequently, the fraction of "isolated" particles (i.e. spherically-shaped and non-agglomerated) is expected to decrease at the expense of the fraction of agglomerated particles. Those changes can be imaged and quantified by a proper analysis of representative TEM images. From this analysis, (i) the number and the surface averaged mean particle size, (ii) the density of isolated and agglomerated nanoparticles, (iii) the total particle density defined as the sum of isolated and agglomerated nanoparticles per μm^2 of the carbon support, (iv) the fraction of agglomerated particles and (v) the percentage of lost isolated particles during the electrochemical treatment, were determined.

We also defined structural markers accessible from electrochemical experiments. In particular, we used "CO stripping" voltammograms as a rapid and facile method to detect *in situ* the agglomeration of the carbon-supported Pt particles. Indeed, it is well established that the presence of Pt nanoparticles featuring surface defects, such as Pt agglomerates, yields a CO electrooxidation pre-peak, which is shifted ca. 50 mV negative *vs.* the CO electrooxidation peak on isolated Pt/C particles [43–47]. Additionally, the position of the main CO stripping peak strongly depends on the mean particle size and shifts toward positive potential when decreasing the Pt particle size [43,44,48].

The relevance of our structural markers is demonstrated in Fig. 1, showing background-subtracted CO stripping voltammograms on Pt/C catalysts with different Pt wt.%, and the associated particle size distributions. As the Pt wt.% increases, the charge under the pre-peak develops, reflecting an increased fraction of agglomerated Pt nanoparticles in the sample. The later agrees with the analysis of TEM images (Table 1). The increased agglomeration degree can be accounted for by considering that, as the metal loading increases, the carbon support cannot accommodate the Pt nanoparticles, and their agglomeration becomes more facile.

At this point of the paper, we would like to point out that caution should be exercised when considering the number of isolated/agglomerated particles listed in Table 1. In particular, our analysis only considered the number and not the size/shape of the Pt agglomerates. Therefore, the relationship with the electrochemical measurements remains to a large extent qualitative but is good enough to draw clear and concise conclusions on the fraction of agglomerated particles present in the sample. In particular, the above results, as well as those obtained by different research groups [43,44,46–49], demonstrate a strong relationship between the amplitude of the pre-peak in CO stripping voltammograms and the extent of particle agglomeration.

3.2. Mobility of Pt crystallites under CO environment

Fig. 2 shows the effect of repetitive CO stripping voltammograms for the different catalysts used in this study. Over the sequence, the CO stripping voltammograms feature a decrease in the charge under the main CO electrooxidation peak at the expense of the charge contained under the pre-peak. Considering the above discussion, these results indicate that the Pt/C nanoparticles are mobile on the high surface area carbon support and agglomerate upon collision. The validity of this assumption is confirmed by the analysis of representative TEM images. Indeed, the latter revealed that the number of isolated particles is reduced in favor of the number agglomerated and/or non-spherical Pt/C nanoparticles, this effect being dependent on the Pt wt. %. This is in agreement with

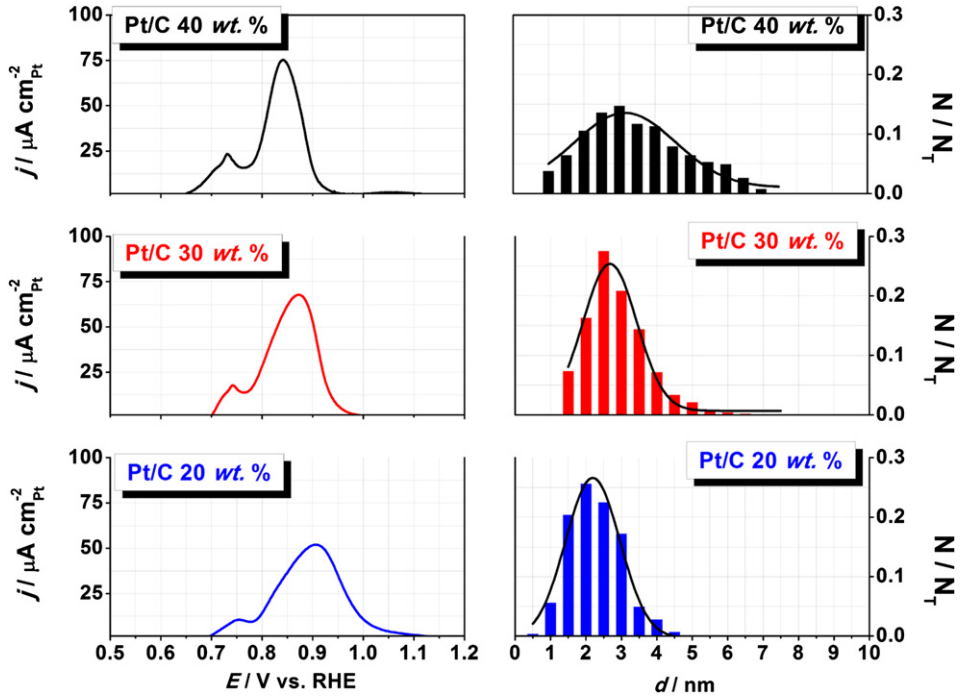

Fig. 1. Average background-subtracted CO stripping voltammograms and particle size distributions of the Pt/C electrocatalysts used in this study. The currents are normalized to the real surface area estimated from CO stripping coulometry. Each voltammogram is the average of three measurements. Electrolyte: 0.1 M $HClO_4$; $v = 0.020$ V s^{-1}; $T = 20$ °C.

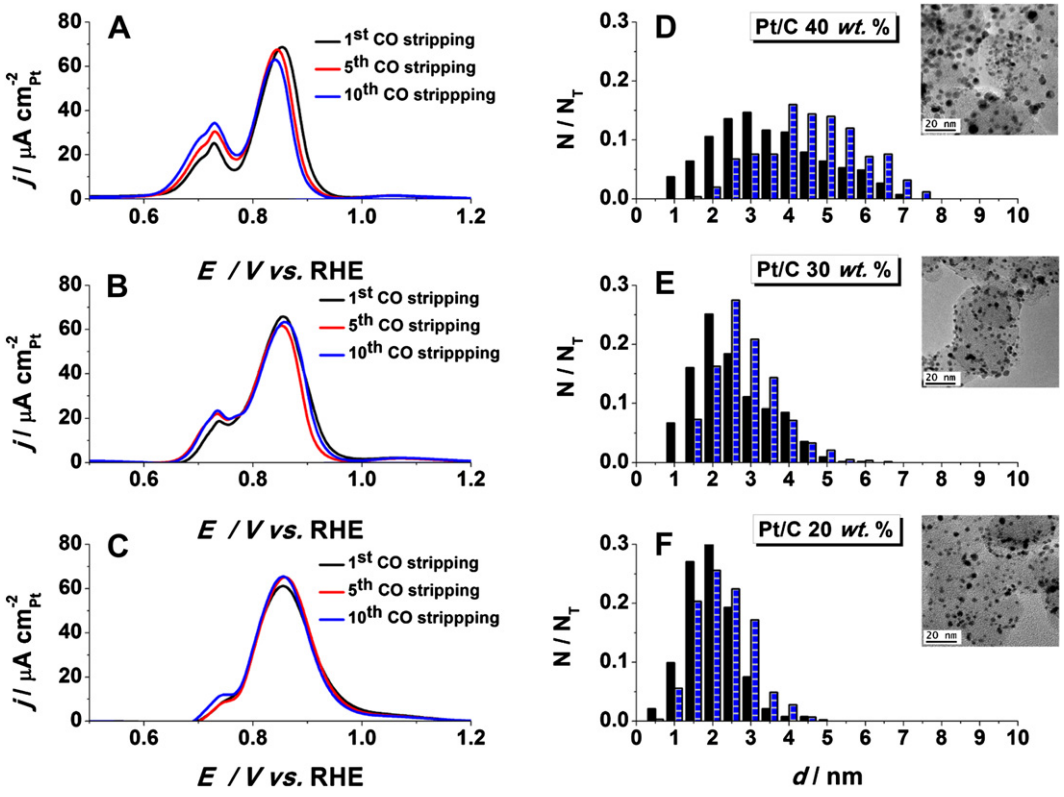

Fig. 2. (A–C) Repetitive background-subtracted CO stripping voltammograms on Pt/C electrocatalysts and (D–F) representative TEM images and particle size distributions of the "isolated" Pt/C particles before (black columns) and after (blue columns) the durability test. The currents are normalized to the real surface area estimated from CO stripping coulometry. Each voltammogram is the average of three measurements. Electrolyte: 0.1 M $HClO_4$; $v = 0.020$ V s^{-1}; $T = 20$ °C. (For interpretation of the references to colour in this figure legend, the reader is referred to the web version of this article.)

theoretical calculations of Ruckenstein et al. that the rate of particle growth is dependent on the metal loading on the support [12].

It is of prime interest to determine whether the morphological changes of the Pt/C nanoparticles are caused by the potential program (potential hold at $E = 0.1$ V *vs.* RHE, i.e. a reducing potential, during 45 min) or by the presence of CO in solution. For that purpose, a sequence of 8 "pseudo CO stripping" voltammograms (consisting of all the steps involved in CO-stripping but using Ar instead of CO) was applied on Pt/C 40 wt.%, and only two "real" CO stripping characterizations were performed at the beginning and at the end of the experiment. Fig. 3 shows the initial and the final CO stripping voltammograms recorded (A) in the presence and (B) in the absence of CO in solution during the 8-cycle sequence. On the right hand side of the figure are also shown representative TEM images as well as the associated particle size distributions. It is clear from Fig. 3B that the potential program causes slight morphological changes, and is not responsible for the agglomeration of the Pt nanoparticles. Indeed, the fraction of isolated and agglomerated particles, and the shape of the particle size distribution are very similar before and after this sequence (Table 1). At variance, when performed in the presence of CO in solution, the sequence of 10 CO stripping voltammograms ($8 + 2$ for characterization) promotes the development of the CO electrooxidation pre-peak, associated with the presence of Pt agglomerates in the sample. In the presence of CO in solution, TEM images revealed considerable loss of "isolated" Pt particles due to the formation of Pt agglomerates.

3.3. Effect of H_2, CO and CH_3OH

Armed with such information, we now investigate the effect of two other molecules hydrogen, and methanol in solution on the morphology of the Pt/C nanoparticles. Fig. 4 shows the CO stripping voltammograms recorded on the fresh Pt/C 40 wt.% before (plain line) and after (dashed line) 50 or 800 CVs in H_2 or CO-saturated solutions or in a solution containing 0.5 M methanol. CO stripping and potential cycling was conducted in different electrochemical cells, referred to as "characterization cell" and "durability test cell" cells, respectively (see Section 2.2). The transfer procedure between the two cells included electrode emersion at $E = 0.1$ V *vs.* RHE, thorough rinsing with MQ-grade water, and transfer to the other cell. The overall procedure takes less than 1 min. For sake of comparison, a "blank" experiment was also performed under argon i.e. in the absence of any reducing molecule in solution. Table 2 shows that the "blank" experiment causes minor morphological changes in the catalyst, with only a slight decrease of the fraction of isolated particles but no increase of the fraction of agglomerated particles. The rationale for such observation is believed to be the detachment of some Pt nanoparticles that has already been observed during accelerated durability tests [50]. Furthermore, the particle size distribution suffered slight changes, which confirms that the observed morphological changes shall be ascribed only to the migration of Pt crystallites (see the particle size distributions in Supplementary material – Figure S1). In CO stripping voltammograms, a slight decrease of the charge under the main CO electrooxidation peak is observed at the benefit of the pre-peak.

At variance, the morphological changes are considerable when H_2, CO or methanol is present in solution during potential cycling. In this case, the charge under the CO electrooxidation pre-peak continuously increases at the expense of the main peak. Representative TEM images of the aged Pt/C catalysts shown in Fig. 4 feature the formation of localized areas of very high Pt loading on Vulcan XC72, while other zones of the carbon support are almost depleted in Pt. The analysis of these images confirms that the fraction of agglomerated particles greatly increases during potential cycling in the presence of H_2, CO or methanol (Table 2 and Fig. 5). The migration rate of Pt crystallites is the largest in CO-containing solution and decreases in the order $CO > CH_3OH > H_2$ (Table 2). To the best of our knowledge, this is the first evidence of Pt crystallite

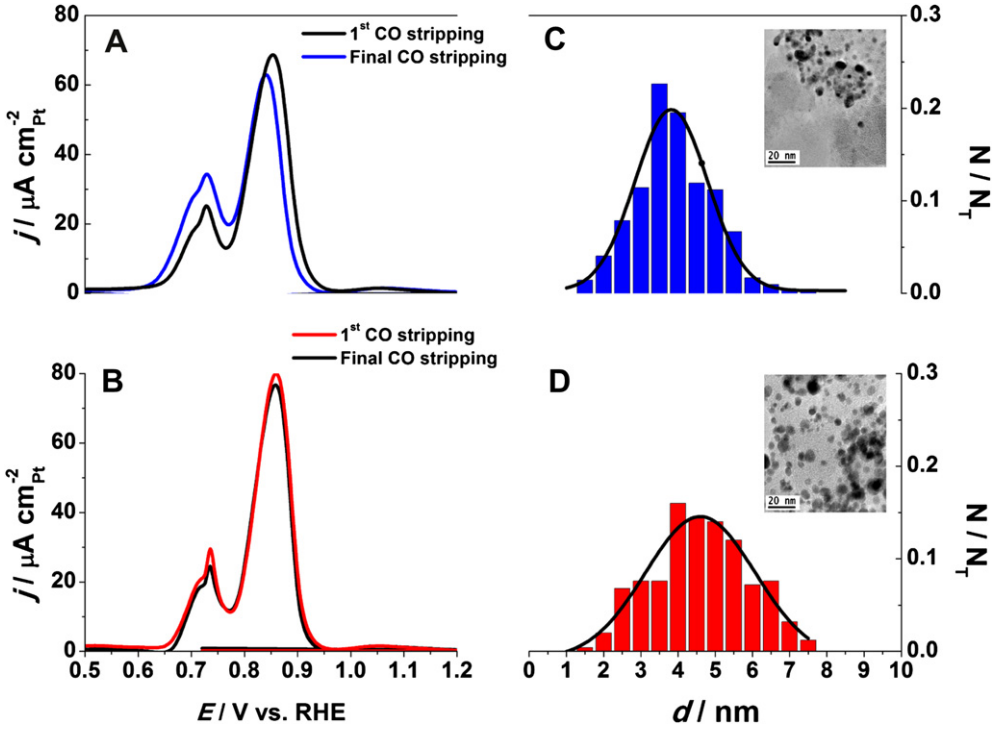

Fig. 3. Initial and final background-subtracted CO stripping voltammograms recorded on Pt/C 40 wt.% (A) in the presence and (B) in the absence of CO in solution during the sequence. (C) and (D) show representative TEM images of the catalyst and the size distributions of the "isolated" particles after each sequence. Electrolyte: 0.1 M $HClO_4$; $v = 0.020$ V s^{-1}; $T = 20$ °C.

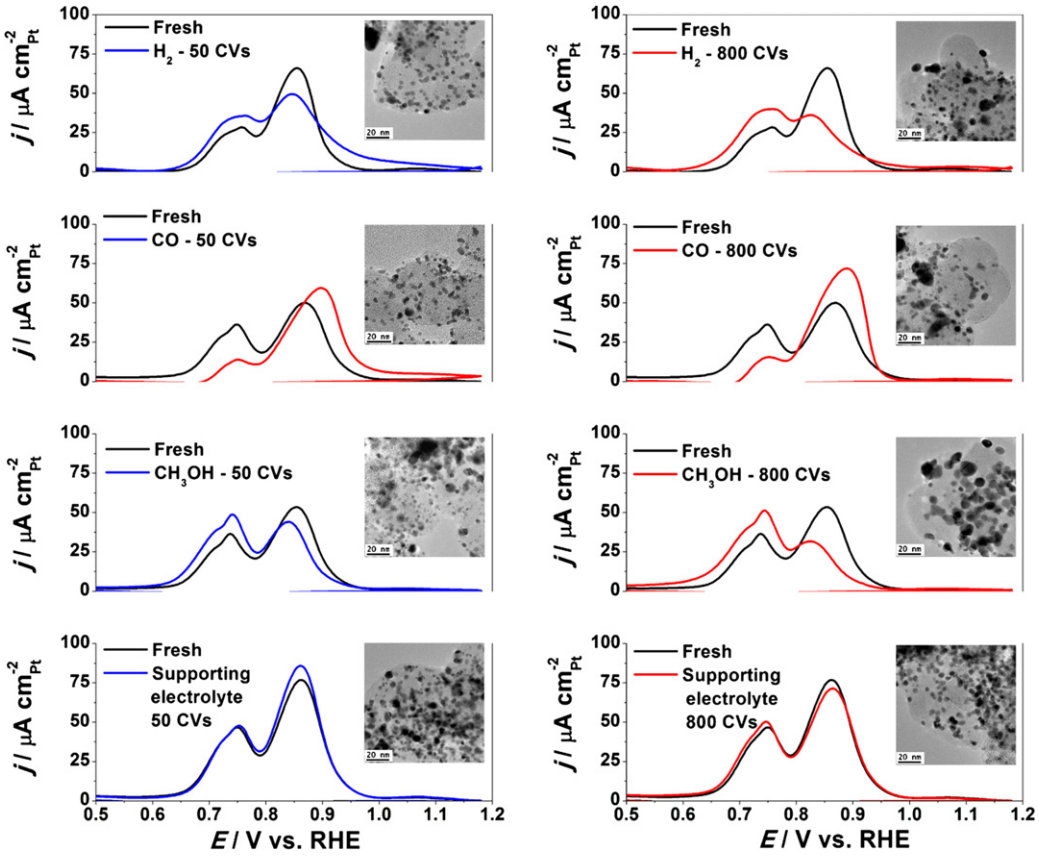

Fig. 4. Background-subtracted CO stripping voltammograms on Pt/C 40 wt.% before/after 50 cycles (left part) or 800 cycles (right part) between 0.05 and 1.23 V *vs.* RHE in electrolyte containing hydrogen, carbon monoxide, methanol or argon. The insets show representative TEM images of the catalyst after 50 or 800 CVs. Electrolyte: 0.1 M $HClO_4$; $\nu = 0.020$ V s^{-1}; $T = 20$ °C.

migration in liquid electrolyte in the absence of other coarsening mechanisms such as Ostwald ripening or carbon corrosion.

We now discuss "bulk CO" experiments where CO is continuously present in solution. In this case, the analysis of representative TEM images clearly show that the presence of CO in solution accelerates the formation of Pt agglomerates. On the other hand, CO stripping voltammograms feature: (i) a decreased charge under the CO electrooxidation pre-peak, and (ii) a shift toward positive electrode potentials of both the onset and the position of the main CO electrooxidation peak. These opposite results can be reconciliated by considering that "surface defects", which are the source of oxygen-containing species necessary to oxidize CO, are removed by potential cycling in CO-containing solution and hence a decreased reactivity for the CO stripping reaction. This effect was first documented by Arenz et al. [51–53].

Estimating the relative contribution of the Pt crystallite migration to the overall Pt surface area loss with respect to other degradation mechanisms is interesting. In the present study, care was taken to avoid experimental conditions favoring Ostwald ripening and carbon corrosion. Consequently, the Pt surface area losses were systematically comprised between 0 and 8%, and are consistent with the evoked migration of Pt crystallites. These percentages are also consistent with high-resolution TEM (HRTEM) images showing that Pt crystallites retain their individual crystallographic characteristics in Pt agglomerates. The latter were found to be composed of individual nanometer-sized crystallites, similar to those found in the fresh sample, and occasionally of sintered single grain coalesced Pt particles.

It is also worth underlying that the formation of localized areas with high Pt loading, such as those imaged in this study, may influence other degradation mechanisms. Indeed, it has been shown that the corrosion rate of the HSAC support is accelerated in the presence of high Pt wt.% [8,37] because highly loaded zones of the carbon support suffer more severe corrosion than the neighboring "Pt-depleted" zones. On the contrary, we point out that the agglomeration/coalescence of Pt nanoparticles may influence positively the rate of 3D Ostwald ripening. Indeed, according to the Gibbs–-Thompson relation, the increase in the mean Pt particle size resulting from the agglomeration of Pt crystallites will cause an increase in their chemical potential, and translate into lower Pt corrosion kinetics [9].

3.4. Effect of the upper potential sweeping conditions

We now investigate the effect of the upper potential limit on the migration of the Pt crystallites. Additional experiments were performed with an upper potential limit $E = 0.40$ V *vs.* RHE so as to avoid the exposure of the Pt/C catalysts to the potential region where surface (hydr)oxides form ($E > 0.60$ V *vs.* RHE, see Ref. [54]). Fig. 6 and Table 3 show that the Pt crystallites remain mobile regardless of the upper potential limit. However, slights changes of the PSD are observed, which confirms that Pt crystallite migration is the only coarsening mechanism at work. Interestingly, a comparison between Tables 2 and 3 shows that the morphological changes of the fresh Pt/C catalyst, although unequivocal, are minored with the decrease of the upper potential limit.

3.5. On the origin of Pt crystallite migration

We now tentatively discuss the origin of the increased mobility of Pt nanoparticles in the presence of H_2, CH_3OH and CO in solution.

Table 2
Number and surface averaged mean particle size, density of isolated and agglomerated particles and loss of isolated Pt particles for a Pt/C 40 wt.% commercial electrocatalyst before/after potential cycling under different atmospheres. HPL stands for high upper potential limit ($0.05 < E < 1.23$ V *vs.* RHE).

Pt/C 40 wt.% E-TeK	Fresh	Supporting electrolyte 50 CVs − HPL	HOR 50 CVs − HPL	MOR 50 CVs − HPL	COOR 50 CVs − HPL	Supporting electrolyte 800 CVs − HPL	HOR 800 CVs − HPL	MOR 800 CVs − HPL	COOR 800 CVs − HPL	ORR 800 CVs − HPL
$\bar{d}_N$/nm	3.5	4.0	3.5	4.5	3.7	4.6	4.4	5.1	5.0	3.3
$\bar{d}_S$/nm	4.5	5.0	4.5	5.4	3.4	6.0	5.7	7.1	5.7	4.3
Number of isolated particles/μm^{-2} carbon	8000	7600	7600	6200	3400	6500	6100	2700	2400	7500
Number of agglomerated particles/μm^{-2} carbon	2600	2500	2500	2600	1700	2400	2400	1800	1400	2400
Total number of particles/μm^{-2} carbon	10,600	10,100	10,100	8800	5100	8900	8500	4500	3800	9900
Loss of isolated particles/%	0	5.0	5.0	22.5	57.5	18.7	23.7	66.2	70.0	6.3

3.5.1. Trapping of Pt nanoparticles at defects of the graphitic crystallites

We first focus on the nature of the sites where Pt nanoparticles are sitting on the HSAC support. During the migration phenomenon, it is believed that Pt crystallites move from a carbon site of lowest energy to another equivalent site without very much expenditure of energy and without any memory of their motions. In an early study, Bett et al. [10] suggested that the edges of the graphitic basal planes may possibly be the sites at which Pt nanoparticles are trapped. Since the density of the "trap" sites is probably limited and characteristic of a carbon support, it is understandable that excessive loading by Pt nanoparticles results in a large fraction of "unstable" Pt nanoparticles (that is in insufficient interaction with the carbon support). Such scenario accounts for the dependence of the rate of Pt crystallite migration on the Pt wt.% observed in Fig. 2 but cannot rationalize the influence of reducing molecules on the process.

3.5.2. Reduction of carbon surface groups

As mentioned in the Introduction, a large variety of CO_{surf} groups exists on high surface area carbon supports but the nature of their interactions with the metal phase remains unclear. Based on X-ray absorption spectroscopy, and attenuated total reflection infrared spectroscopy results, Hull et al. [32] convincingly showed that Pt nanoparticles interact with carbon nanotubes via ester and carboxyl oxygen atoms. Strong interactions between the metal phase and the oxygen-bearing surface groups find also support in the work of Antonucci et al. [19]. The authors reported an increase in the Pt_{4f} binding energy with the increase of the concentration of acidic carbon surface oxides. Therefore, it is not surprising that the presence of reducing molecules in solution enhances the rate of Pt crystallite migration. Indeed, these molecules all possess a standard potential close to 0 V *vs.* SHE: (i) H_2 ($E^0_{H^+/H_2} = 0.00$ V *vs.* SHE), (ii) CH_3OH ($E^\circ_{CO_2/CH_3OH/} = 0.04$ V *vs.* SHE) and (iii) CO ($E^\circ_{CO_2/CO} = -0.10$ V *vs.* SHE), i.e. possess great ability to reduce the carbon surface oxides ($E^\circ_{CO/C} = 0.52$ V *vs.* SHE) [55]. The reduction of the oxygen-bearing groups present on the surface of the Vulcan XC72 support weakens the interaction with the Pt nanoparticles, and hence facilitates the mobility and further collision of these nanocrystals. Keeping the same idea in mind, it is striking to note that the rate at which Pt crystallites are lost is the fastest (see Table 2) when CO is present in solution, that for the most negative value of the Gibbs energy of the reaction ΔG. The reduction of oxygen-bearing groups of the carbon support by H_2, CO or CH_3OH molecules is also documented in the literature. Indeed, in a temperature-programmed reduction and temperature-programmed desorption study, Roman-Martinez et al. [56] evidenced that H_2 assists the desorption and the reduction of carboxylic acid anhydride- and quinone-containing groups into water. Obviously, the experimental conditions are largely different in the study of Roman-Martinez (gas phase, elevated temperatures) and in our study (liquid electrolyte, strong electric field, low temperatures) but a closer look to background-subtracted CO stripping voltammograms in Fig. 7 shows that the same phenomena may occur under polarization. Indeed, a negative current is observed in the background-subtracted CO stripping voltammogram at around $0.60 < E < 0.70$ V *vs.* RHE, which is a potential zone where electrons are transferred on quinone/hydroquinone groups [1] or pyrone-like structures (combination of non-neighboring carbonyl and ether oxygen atoms at the edge of the graphene layers) [57]. Such feature strongly suggests that extended polarization at low electrode potential in the presence of CO reduces part of the CO_{surf} groups. Consequently, an increased oxidation current is observed on the first positive-going potential scan, and results in the negative current in the

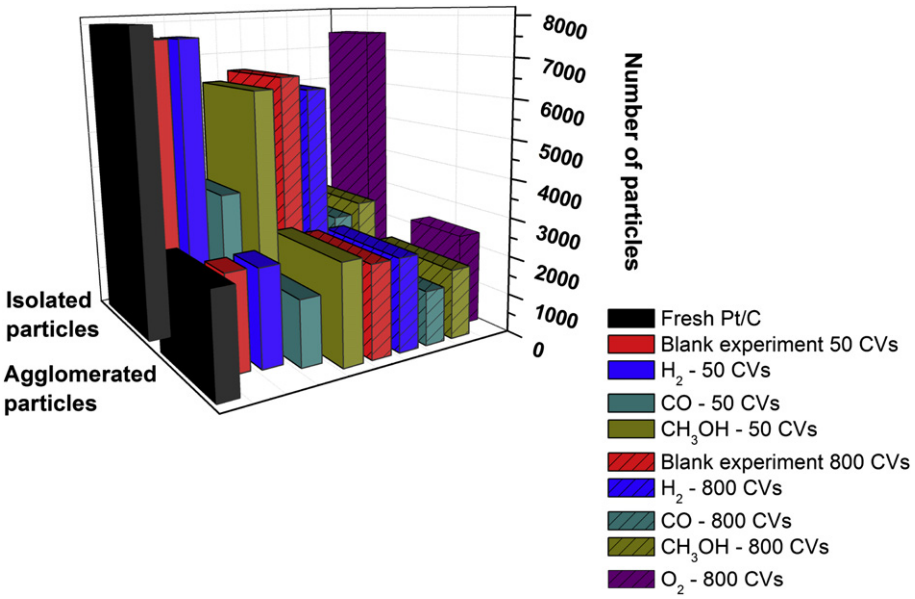

Fig. 5. The number of isolated and agglomerated particles per μm^2 of carbon before/after potential cycling in electrolyte containing hydrogen, carbon monoxide, methanol or argon.

background-subtracted CO stripping voltammograms. The above hypothesis has also been confirmed recently by *in situ* infrared spectroscopy experiments and will be the subject of forthcoming publication.

Keeping this idea in mind, we also performed potential cycling in O_2-containing solution, all other experimental conditions being kept identical as in Fig. 4. Fig. 8 shows that the shape of the CO stripping voltammograms remains largely unchanged during the durability test, which confirms that the migration of the Pt crystallites is restricted in oxidizing conditions (promoting the persistence of CO_{surf} groups on the carbon surface). Also, the analysis of TEM images confirms that the

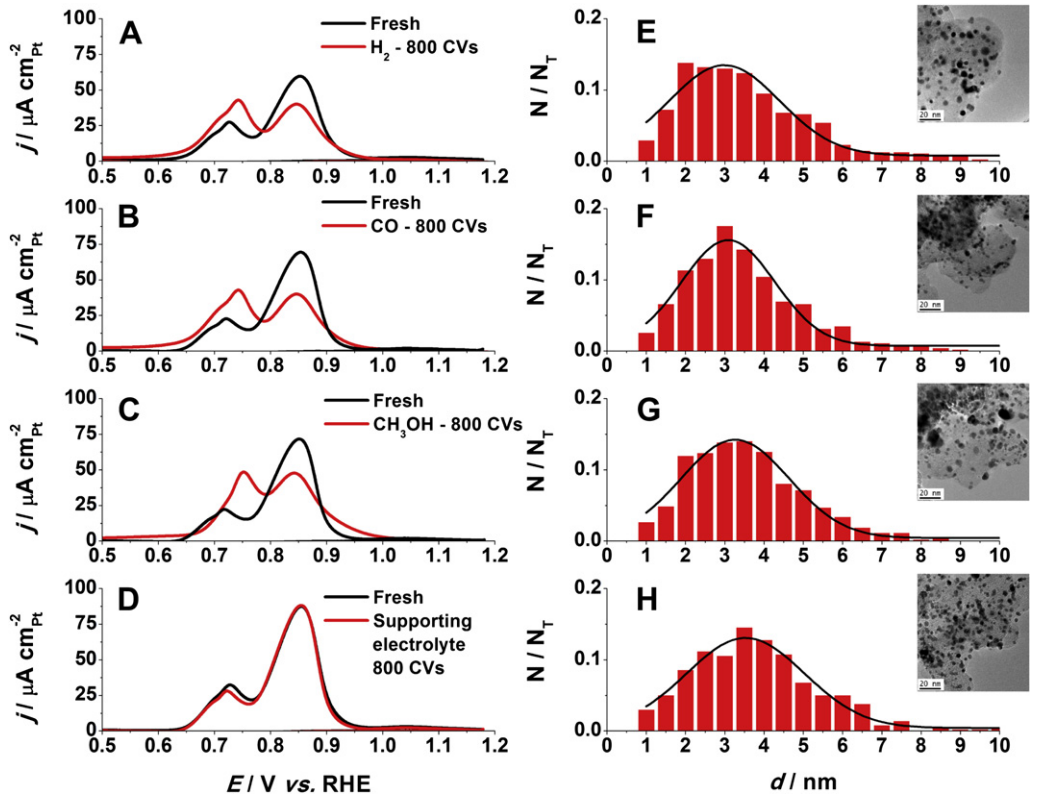

Fig. 6. (A–D) Background-subtracted CO stripping voltammograms and (E–H) particle size distribution of Pt/C catalysts before/after 800 cycles between 0.05 and 0.40 V *vs.* RHE in electrolyte containing hydrogen, carbon monoxide, methanol or argon. The insets show representative TEM images of the Pt/C catalysts and the size distributions of the "isolated" particles after the 800 cycles. Electrolyte: 0.1 M $HClO_4$; $v = 0.020$ V s^{-1}; $T = 20$ °C.

Table 3
Number and surface averaged mean particle size, density of isolated and agglomerated particles and loss of isolated Pt particles for a Pt/C 40 wt.% commercial electrocatalyst before/after potential cycling in various conditions. LPL stands for low potential limit ($0.05 < E < 0.40$ V *vs.* RHE).

Pt/C 40 wt.% E-TeK	Supporting electrolyte 800 CVs – LPL	HOR 800 CVs – LPL	MOR 800 CVs – LPL	COOR 800 CVs – LPL
$\overline{d}_N$/nm	3.8	3.6	5.1	3.5
$\overline{d}_S$/nm	5.0	5.2	7.1	4.7
Number of isolated particles/μm^{-2} carbon	6500	6400	4800	5400
Number of agglomerated particles/μm^{-2} carbon	2400	2500	2500	2300
Total number of particles/μm^{-2} carbon	8900	8900	7300	7700
Loss of isolated particles/%	27.0	28.0	34.2	29.9

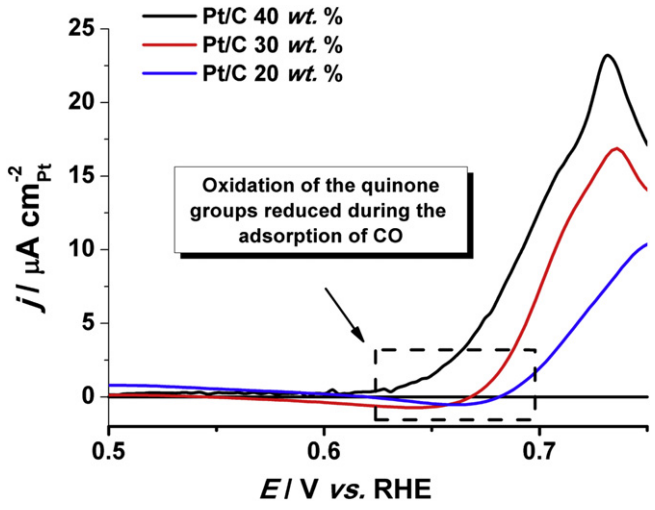

Fig. 7. Background-subtracted CO stripping voltammograms performed on different Pt/C electrocatalysts. The negative current in the potential region $0.60 < E < 0.70$ V *vs.* suggests that CO_{surf} groups were at least partially reduced during the adsorption of CO at $E = 0.1$V *vs.* RHE. Each voltammogram is the average of three measurements. Electrolyte: 0.1 M $HClO_4$; $v = 0.020$ V s^{-1}; $T = 20$ °C.

coarsening of the Pt nanoparticles is kept to a low extent (Table 2). Here again, the parallel with gas-phase catalysis is striking. Indeed, Sellin et al. [58] exposed Vulcan XC72-supported Pt nanoparticles to heat-treatment at $T = 573$ K under oxidizing, inert, and reducing atmospheres. They reported the agglomeration of the Pt crystallites and an increase of the mean crystallite size under 3% H_2/He, whereas little structural changes were detected under air.

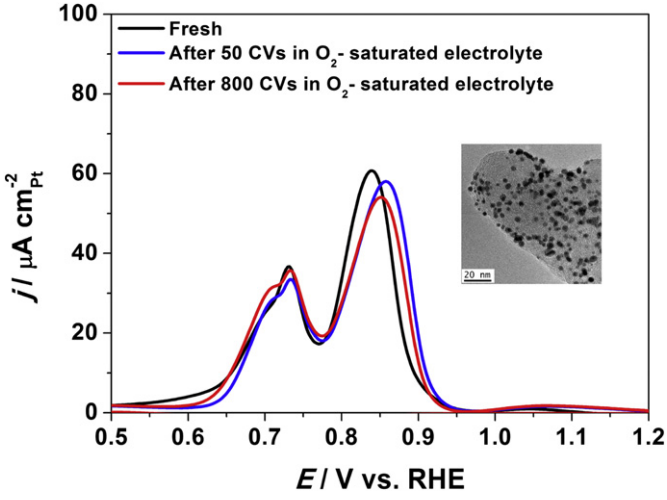

Fig. 8. Background-subtracted CO stripping voltammograms recorded on Pt/C 40 wt.% before/after 50 and 800 cycles between 0.05 and 1.23 V *vs.* RHE in oxygen-saturated electrolyte. The inset shows a representative TEM image of the Pt/C catalyst after the 800 potential cycles. Electrolyte: 0.1 M $HClO_4$; $v = 0.020$ V s^{-1}; $T = 20$ °C.

4. Conclusions

The results presented in this study evidenced that Pt crystallites are not immobile on an HSAC support but can collide and agglomerate under potential cycling conditions. Although bearing minor importance in terms of Pt surface area losses, this phenomenon may influence or even accelerate the rate of other degradation mechanisms, such as the electrochemical corrosion of the carbon support and the 3D Ostwald ripening. The migration rate of the Pt crystallites is the largest in CO-containing solution and decreases in the order $CO > CH_3OH > H_2$. We postulate that the morphological changes of the Pt/C nanoparticles are related to the reduction of the oxygen-bearing surface groups strongly interacting with the Pt nanocrystallites.

Appendix A. Supplementary material

Supplementary material associated with this article can be found, in the online version, at http://dx.doi.org/10.1016/j.jpowsour.2012.06.016.

References

[1] K. Kinoshita, Carbon, Electrochemical and Physicochemical Properties, John Wiley & Sons, New York, 1988.
[2] F. Maillard, P. Simonov, E.R. Savinova, in: P. Serp, J.L. Figueiredo (Eds.), Carbon Materials for Catalysis, John Wiley & Sons, Inc., New York, 2009, pp. 429–480.
[3] L. Dubau, F. Maillard, M. Chatenet, L. Guétaz, J. André, E. Rossinot, J. Electrochem. Soc. 157 (2010) B1887–B1895.
[4] L. Dubau, J. Durst, F. Maillard, M. Chatenet, L. Guétaz, J. André, E. Rossinot, Electrochim. Acta 56 (2011) 10658–10667.
[5] L. Dubau, F. Maillard, M. Chatenet, J. André, E. Rossinot, Electrochim. Acta 56 (2010) 776–783.
[6] L. Dubau, J. Durst, F. Maillard, M. Chatenet, L. Guétaz, J. André, E. Rossinot, Fuel Cells 12 (2011) 188–198.
[7] E. Guilminot, A. Corcella, F. Charlot, F. Maillard, M. Chatenet, J. Electrochem. Soc. 154 (2007) B96–B105.
[8] L.M. Roen, C.H. Paik, T.D. Jarvi, Electrochem. Solid-State Lett. 7 (2004) A19–A22.
[9] Y. Shao-Horn, W. Sheng, S. Chen, P. Ferreira, E. Holby, D. Morgan, Top. Catal. 46 (2007) 285–305.
[10] J.A. Bett, K. Kinoshita, P. Stonehart, J. Catal. 35 (1974) 307–316.
[11] J.A.S. Bett, K. Kinoshita, P. Stonehart, J. Catal. 41 (1976) 124–133.
[12] E. Ruckenstein, B. Pulvermacher, J. Catal. 29 (1973) 224–245.
[13] P.J. Ferreira, G.J. la O', Y. Shao-Horn, D. Morgan, R. Makharia, S. Kocha, H.A. Gasteiger, J. Electrochem. Soc. 152 (2005) A2256–A2271.
[14] E. Guilminot, A. Corcella, C. Iojoiu, G. Berthomé, F. Maillard, M. Chatenet, J.-Y. Sanchez, J. Electrochem. Soc. 154 (2007) B1106–B1114.
[15] M.S. Wilson, F.H. Garzon, K.E. Sickafus, S. Gottesfeld, J. Electrochem. Soc. 140 (1993) 2872–2877.
[16] P. Ehrburger, O.P. Mahajan, P.L. Walker Jr., J. Catal. 43 (1976) 61–67.
[17] D.R. Lowde, J.O. Williams, P.A. Attwood, R.J. Bird, B.D. McNicol, R.T. Short, J. Chem. Soc. Faraday Trans. 75 (1979) 2312.
[18] C. Prado-Burguete, A. Linares-Solano, F. Rodriguez-Reinoso, C.S.-M. de Lecea, J. Catal. 115 (1989) 98–106.

[19] P.L. Antonucci, V. Alderucci, N. Giordano, D.L. Cocke, H. Kim, J Appl. Electrochem. 24 (1994) 58–65.
[20] S. Adora, Y. Soldo-Olivier, R. Faure, R. Durand, E. Dartyge, F. Baudelet, J. Phys. Chem. B 105 (2001) 10489–10495.
[21] F. Coloma, A. Sepulveda-Escribano, J.L.G. Fierro, F. Rodriguez-Reinoso, Langmuir 10 (1994) 750–755.
[22] S.R. de Miguel, O.A. Scelza, M.C. Roman-Martinez, C. Salinas-Martinez de Lecea, D. Cazorla-Amoros, A. Linares-Solano, Appl. Catal. A 170 (1998) 93–103.
[23] A. Guerrero-Ruiz, P. Badenes, I. Rodriguez-Ramos, Appl. Catal. A 173 (1998) 313–321.
[24] M.C. Roman-Martinez, D. Cazorla-Amoros, A. Linares-Solano, C.S.-M. De Lecea, H. Yamashita, M. Anpo, Carbon 33 (1995) 3–13.
[25] G.C. Torres, E.L. Jablonski, G.T. Baronetti, A.A. Castro, S.R. de Miguel, O.A. Scelza, M.D. Blanco, M.A. Peña Jiménez, J.L.G. Fierro, Appl. Catal. A 161 (1997) 213–226.
[26] L.J. Hillenbrand, J.W. Lacksonen, J. Electrochem. Soc. 112 (1965) 249–252.
[27] J. Escard, C. Leclère, J.P. Contour, J. Catal. 29 (1973) 31–39.
[28] A.K. Shukla, A. Hamnett, A. Roy, S.R. Barman, D.D. Sarma, V. Alderucci, L. Pino, N. Giordano, J. Electroanal. Chem. 352 (1993) 337–343.
[29] A.K. Shukla, M.K. Ravikumar, A. Roy, S.R. Barman, D.D. Sarma, A.S. Arico, V. Antonucci, L. Pino, N. Giordano, J. Electrochem. Soc. 141 (1994) 1517–1522.
[30] V. Alderucci, L. Pino, P.L. Antonucci, W. Roh, J. Cho, H. Kim, D.L. Cocke, V. Antonucci, Mater. Chem. Phys. 41 (1995) 9–14.
[31] F. Coloma, A. Sepulveda-Escribano, J.L.G. Fierro, F. Rodriguez-Reinoso, Appl. Catal. A 148 (1996) 63–80.
[32] R.V. Hull, L. Li, Y.C. Xing, C.C. Chusuei, Chem. Mater. 18 (2006) 1780–1788.
[33] J. Petroski, M.A. El-Sayed, J. Phys. Chem. A 107 (2003) 8371–8375.
[34] F. Coloma, A. Sepulveda-Escribano, F. Rodriguez-Reinoso, J. Catal. 154 (1995) 299–305.
[35] W.M. Chen, B.D. Qu, Int. J. Hydrogen Energy 35 (2010) 10102–10108.
[36] K. Kinoshita, J.A.S. Bett, Carbon 12 (1974) 525–533.
[37] F. Maillard, A. Bonnefont, F. Micoud, Electrochem. Commun. 13 (2011) 1109–1111.
[38] C.C. Hung, P.Y. Lim, J.R. Chen, H.C. Shih, J. Power Sources 196 (2011) 140–146.
[39] N. Giordano, P.L. Antonucci, E. Passalacqua, L. Pino, A.S. Arico, K. Kinoshita, Electrochim. Acta 36 (1991) 1931–1935.
[40] J. Willsau, J. Heitbaum, J. Electroanal. Chem. 161 (1984) 93–101.
[41] K.H. Kangasniemi, D.A. Condit, T.D. Jarvi, J. Electrochem. Soc. 151 (2004) E125–E132.
[42] K. Kinoshita, J. Bett, Carbon 11 (1973) 237–247.
[43] F. Maillard, S. Schreier, M. Hanzlik, E.R. Savinova, S. Weinkauf, U. Stimming, Phys. Chem. Chem. Phys. 7 (2005) 385–393.
[44] F. Maillard, E.R. Savinova, U. Stimming, J. Electroanal. Chem. 599 (2007) 221–232.
[45] O.V. Cherstiouk, A.N. Gavrilov, L.M. Plyasova, I.Y. Molina, G.A. Tsirlina, E.R. Savinova, J. Solid State Electrochem. 12 (2008) 497–509.
[46] E.G. Ciapina, S.F. Santos, E.R. Gonzalez, J. Electroanal. Chem. 644 (2010) 132–143.
[47] A. Lopez-Cudero, J. Solla-Gullon, E. Herrero, A. Aldaz, J.M. Feliu, J. Electroanal. Chem. 644 (2010) 117–126.
[48] F. Maillard, M. Eikerling, O.V. Cherstiouk, S. Schreier, E. Savinova, U. Stimming, Faraday Discuss. 125 (2004) 357–377.
[49] O.V. Cherstiouk, P.A. Simonov, E.R. Savinova, Electrochim. Acta 48 (2003) 3851–3860.
[50] K.J.J. Mayrhofer, S.J. Ashton, J.C. Meier, G.K.H. Wiberg, M. Hanzlik, M. Arenz, J. Power Sources 185 (2008) 734–739.
[51] M. Arenz, K.J.J. Mayrhofer, V. Stamenkovic, B.B. Blizanac, T. Tomoyuki, P.N. Ross, N.M. Markovic, J. Am. Chem. Soc. 127 (2005) 6819–6829.
[52] K.J.J. Mayrhofer, M. Arenz, B.B. Blizanac, V.R. Stamenkovic, P.N. Ross, N.M. Markovic, Electrochim. Acta 50 (2005) 5144–5154.
[53] D.S. Strmcnik, D.V. Tripkovic, D. van der Vliet, K.C. Chang, V. Komanicky, H. You, G. Karapetrov, J. Greeley, V.R. Stamenkovic, N.M. Markovic, J. Am. Chem. Soc. 130 (2008) 15332–15339.
[54] B. Andreaus, F. Maillard, J. Kocylo, E.R. Savinova, M. Eikerling, J. Phys. Chem. B 110 (2006) 21028–21040.
[55] CRC Handbook of Chemistry and Physics, Internet Version 2005, CRC Press, 2005.
[56] M.C. Román-Martínez, D. Cazorla-Amorós, A. Linares-Solano, C.S.-M. de Lecea, Carbon 31 (1993) 895–902.
[57] M.A. Montes-Morán, D. Suárez, J.A. Menéndez, E. Fuente, Carbon 42 (2004) 1219–1225.
[58] R. Sellin, C. Grolleau, S. Arrii-Clacens, S. Pronier, J.M. Clacens, C. Coutanceau, J.M. Léger, J. Phys. Chem. C 113 (2009) 21735–21744.